*Physicochem. Probl. Miner. Process., 59(6), 2023, 174897*

http://www.journalssystem.com/ppmp

Physicochemical Problems of Mineral Processing

ISSN 1643-1049


# Semi-quantitative analysis study of the impact of microwave treatment on fly ash

**Xian Yun Ma [1,2], Yi Miao Nie [1,2], Jia Le Guo [1,2], Yang Chen [1,2], Zhen Jia Chang [1,2], Ling Wang [1,2], Shu Xian Liu [1,2], Long Wang [1,2,3]**

[1] College of Mining Engineering, North China University of Science and Technology, Tangshan 063210, China

[2] Hebei Province Key Laboratory of Mining Exploitation and Security Technology, Tangshan 063210, China

[3] State Key Laboratory of Clean Utilization of Complex Nonferrous Metal Resources, Kunming 650093, China

Corresponding author: nieym168@163.com (Yi Miao Nie)

**Abstract:** Pre-processing provides an effective way for fly ash's high value-added utilization. However, the shortcomings of pre-processing methods such as grinding and flotation are apparent with many disadvantages that make it more challenging to use efficiently. Microwave heating helps the $SiO_2$-$Al_2O_3$ bond break, not only can make the structural change of the material can also promote the chemical reaction process. In the article, XRD, SEM, FT-IR, ammonia nitrogen adsorption, and other methods were used to analyze the changes in the properties of fly ash before and after microwave pre-treatment, the change in adsorption performance of fly ash before and after microwave treatment was analyzed. The study found that under microwave conditions of 600 W and 15 min, the adsorption rate of ammonia nitrogen by fly ash reached a maximum of 29.67%. The intensity of mullite and amorphous diffraction peaks decreased after 20 min at 600 W. The Si-O-(Si, Al) and Si-O-(Si) bonds showed significant changes at 15 min and 20 min under 600 W conditions. Based on the results, the microwave conditions were selected at 600 W for different periods, and semi-quantitative analysis was carried out by XRD-Rietveld, infrared peak fitting, and nuclear magnetic resonance. The XRD-Rietveld analysis showed that the amorphous phase content reached 46.18% at 15 min. In the infrared peak fitting, the fitting area at 1300-900 $cm^{-1}$ and 600-400 $cm^{-1}$ peaks at 56.92% at 25 min and 17.5% at 15 min, respectively. The silicon-oxygen network's degree of connection and polymerization was reduced after 15 min of microwave treatment for the nuclear magnetic resonance analysis. By combining specific surface area measurements, it was discovered that the maximum specific surface area attained a value of 3.122 $m^2/g$ at 15 min.

***Keywords:*** microwave, fly ash, semi-quantitative analysis, adsorption, XRD refinement, infrared fitting, NMR

## 1. Introduction

The increasing accumulation of fly ash has engendered significant land occupation and caused environmental pollution. It is an attractive way to refine fly ash from a wide range of low-priced sources into a valuable resource through specialized processing (Mathapati et al., 2021; Ma et al., 2022; Valeev et al., 2022; Das et al., 2023). Fly ash contains many valuable elements such as silicon, aluminium, iron, carbon, gallium, and germanium. Extracting valuable elements from fly ash is a meaningful way to realize the high value-added utilization of fly ash. The chemical composition of fly ash is similar to clay and a mixture of volcanic ash. Under certain conditions, fly ash can react with water, forming a cementitious material resembling cement in strength, which can be used in building materials. Applying fly ash in agriculture mainly improves the clay and acid soil by improving the soil's physical and chemical properties. Fly ash has a specific adsorption capacity and can be used as an adsorbent or catalyst in environmental engineering to treat wastewater and waste gas (Dindi et al., 2019; Um et al., 2021; Majid., 2021; Nguyen et al., 2023; Rusănescu et al., 2023). However, low content of active components, high thermal stability, and poor formability limit the application and effectiveness of fly

DOI: 10.37190/ppmp/174897

ash. Therefore, improving the activity and performance of fly ash has become the focus of current research (Ma et al., 2021).

Physical and chemical pretreatment is generally used to improve the activity of fly ash. Physical pretreatment refers to crushing glass particles without changing their chemical composition, increasing the specific surface area, and destroying the compact structure of glass, increasing the contact area between fly ash and pollutants to improve the adsorption capacity, thereby improving the activity of fly ash. In contrast, chemical pretreatment stimulates the activity of fly ash by changing the chemical composition and destroying the stable crystal structure of mullite and other phases (Moisili et al., 2022). However, various pretreatment methods have their limitations. For example, grinding methods are limited in enhancing mobility; gravity concentration is unsuitable for fine particles; flotation causes water resource waste; magnetic separation has low efficiency; high pressure requires advanced equipment requirements; and calcination leads to secondary pollution (Nguyen et al., 2021). Microwave pretreatment technology boasts the advantages of rapidity, efficiency, and environmental friendliness. Using microwave radiation can alter materials' physical and chemical properties by heating and evaporating their water molecules (Zhang et al., 2020). Research has demonstrated that microwave pretreatment can increase the reactivity in fly ash while enhancing its fluidity and dispersibility, thereby augmenting its application value (Shi et al., 2023). The application of microwave treatment to fly ash is an innovative approach that enhances the total utilization value of fly ash, promotes the resource utilization of industrial waste, and mitigates environmental pollution. (Gopalan et al., 2022). Revising the activity of fly ash was improved by microwave pretreatment and semi-quantitative analysis was conducted by XRD, FT-IR, and NMR is of great practical significance and application prospects in promoting the resource utilization of fly ash and mitigating environmental pollution (Panitsa et al., 2022). Herein, a semi-quantitative analysis was performed to investigate the effects of microwave treatment on fly ash. It aimed to identify optimal microwave treatment conditions through this analysis of the effects of microwave treatment to obtain superior results. Additionally, we analyze the microwave energy that causes the fracture of the $SiO_2$-$Al_2O_3$ bond of fly ash, resulting in the change of properties in fly ash properties before and after microwave treatment, further examining the degree and mechanism of influence that microwaves have on fly ash.

## 2. Materials and methods

### 2.1. Materials

The fly ash sample used in this study was obtained from a Tangshan City, Hebei Province power plant, in China. The chemical composition of the sample was determined by chemical titration (Lv et al., 2018), and the results are presented in Table 1. The contents of $SiO_2$, $Al_2O_3$, $Fe_2O_3$, and CaO of the sample were 49.94%, 30.24%, 4.54%, and 4.06%, respectively. According to ASTMC618 (Han et al., 2003), the fly ash could be classified as grade F class fly ash with ($SiO_2$ + $Al_2O_3$+ $Fe_2O_3$)>70% (Zhou et al., 2022).

Table 1. Chemical composition of fly ash raw material

| Composition | $SiO_2$ | $TiO_2$ | CaO | MgO | $Al_2O_3$ | $K_2O$ | $Na_2O$ | $Fe_2O_3$ | MnO | C | Other |
|---|---|---|---|---|---|---|---|---|---|---|---|
| Mass fraction (%) | 49.94 | 1.14 | 4.06 | 0.78 | 30.24 | 1.00 | 0.14 | 4.54 | 0.084 | 6.41 | 1.686 |

The results for the XRD and SEM morphology analyses of the sample are shown in Figs. 1 and 2, respectively. Fig. 1 shows the "peak" in the 2θ range of 15~30° corresponds to the glassy phase material present in fly ash, which produces activity in the fly ash. The primary crystalline phases include fly ash mullite and quartz (Gultekin et al., 2023). Fig. 2 shows that fly ash has many spherical particles of different sizes, and the surface is smooth. The spherical material was the amorphous glass phase of fly ash. The granular material attached to the glass surface and the mass of material around the glass consisted of crystalline substances (quartz and mullite).

### 2.2. Experimental details

The screened fly ash was used as the experimental sample, and the microwave treatment was carried out at 400 W, 500 W, 600 W, 700 W, 800 W, and at 10 min, 15 min, 20 min, 25 min, and 30 min,

respectively. In the microwave high-temperature muffle furnace, the microwave frequency was 2450 MHz.

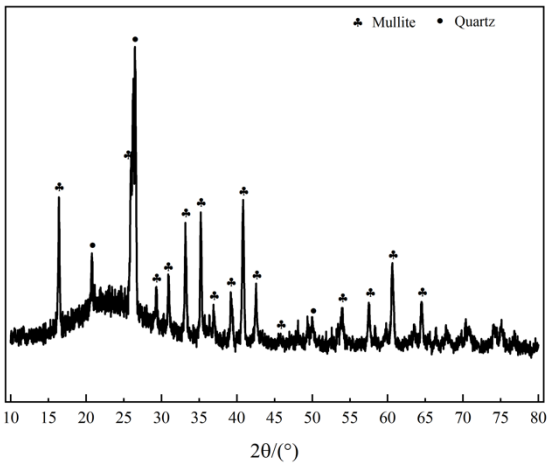


Fig. 1. XRD patterns of fly ash

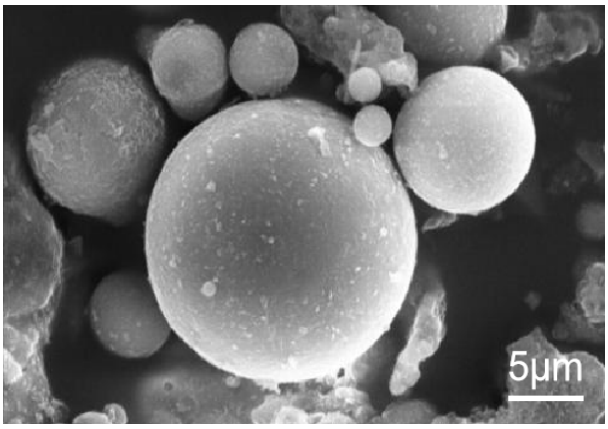


Fig. 2. SEM morphology of fly ash

### 2.3. Experimental details

The screened fly ash was used as the experimental sample, and the microwave treatment was carried out at 400 W, 500 W, 600 W, 700 W, 800 W, and at 10 min, 15 min, 20 min, 25 min, and 30 min, respectively. In the microwave high-temperature muffle furnace, the microwave frequency was 2450 MHz.

The untreated 0.2 g fly ash was treated under different microwave conditions for adsorption experiment and put into a simulated ammonia nitrogen wastewater prepared from ammonium chloride with a concentration of 10 mg/dm$^3$ and adsorbed for 0.5 h under a magnetic agitator at 20°C and a rotating speed of 200 rpm (Praipipat et al., 2023). After the adsorption, the solid and liquid were separated by pumping and filtration. The absorbance was measured by 722 s spectrophotometer, the absorption wavelength was 420 nm and the absorbance curve of standard solution was established to test the adsorption rate. Among them, the adsorption rate of untreated fly ash was 1.02%.

A semi-quantitative analysis of fly ash before and after treatment was carried out using the XRD-Rietveld refinement, infrared analysis, and nuclear magnetic resonance (Yildiz et al., 2020). The Rietveld method can refine XRD patterns and calculate the relative content of each phase in the sample. This method consists of two main steps: phase identification and whole pattern fitting. The phase identification is performed using Jade software, identifying the main crystalline phases in the raw fly ash as mullite and quartz. The pattern fitting uses the advanced Rietveld method and the phase identification results. The experimental pattern is fitted to the calculated one, and the intensities of the diffraction peaks are used to calculate the relative content of each crystalline phase. However, this

method only allows for calculating the relative content of crystalline phases, making it necessary to use a standard internal method to compare and calculate the content of amorphous phases. This method can effectively determine the content of amorphous phases and improve the accuracy of sample analysis. Origin2022 software was used for infrared spectroscopic analysis to compare the molecular vibration information of fly ash particles under different microwave conditions within the wavenumber range of 1300-400 $cm^{-1}$ and performed peak fitting (Zuma et al., 2021). The flow chart of the experimental method is shown in Fig. 3.

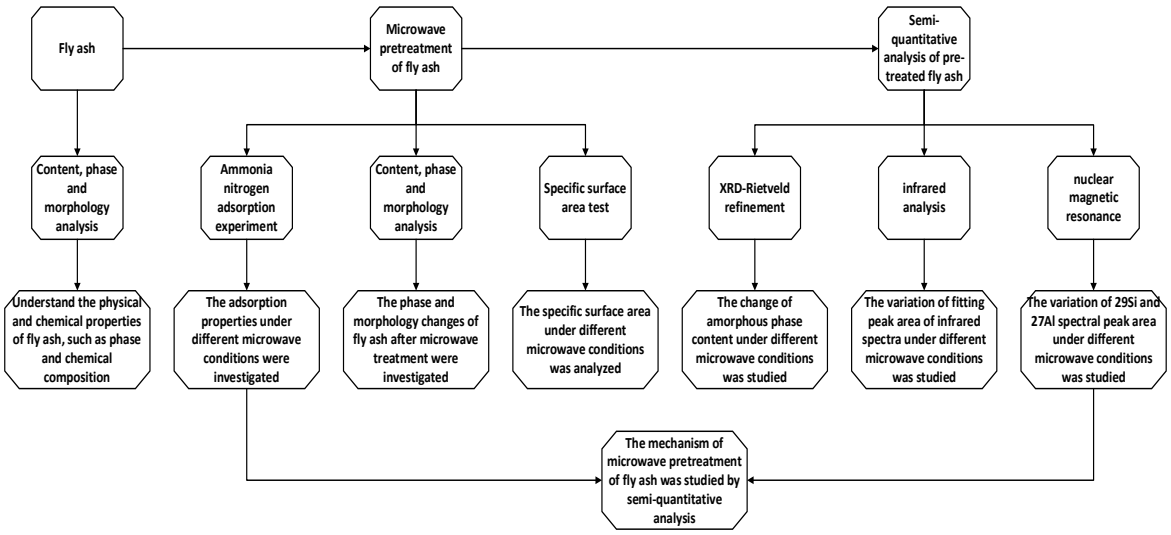


Fig. 3. Experimental flow chart

### 2.4. Characterization of samples

This study used a D/MAX2500PC X-ray diffractometer (XRD) to perform phase analysis on microwave-treated fly ash. The testing conditions were 40 kV voltage, 100 mA current, Cu target material, 8°/min scan speed, and a scanning angle range of 10-80°. Before analyzing the sample morphology using an S-4800 focused ion beam scanning electron microscope (SEM), it was necessary to use a gold-palladium mixture sputter coating to reduce harmful charge interference. In addition, Thermo Scientific Nicolet iS20 Fourier transforms infrared spectrometer (FTIR) was used to analyze the chemical groups on the surface of fly ash. Before conducting the infrared spectroscopy test, the sample must be dried to remove the influence of moisture and pressed into pellets after adding KBr, for scanning in the wavenumber range of 4000-400 $cm^{-1}$. JW-BK112 specific surface area analyzer was used to measure the specific surface area and pore size. Agilent 600 M spectrometer (NMR) recorded solid-state $^{29}Si$ DD/MAS NMR spectra at a resonance frequency of 199.13 MHz, using dipolar and high-power 1H decoupling (Chen et al., 2022). The powder sample was placed in a 40 mm pencil-type zirconia rotor. The spectrum was obtained at a rotation speed of 8 kHz (4 μs 90° pulse), with a 3.6 μs recycle delay and a 5 s acquisition time. The Si signal of tetramethylsilane (TMS) at 0ppm was used as the reference for the $^{29}Si$ chemical shift. The number of scans was 4000. $^{27}Al$ MAS NMR spectra were recorded on an Agilent 600 M spectrometer, operating for 1 hour at a Larmor frequency of 600 MHz. A 4.0 mm double-resonance 1H-XMAS probe was used with a rotation frequency of 8 kHz. The $^{27}Al$ experiment was performed at a Larmor frequency of 156.25 MHz. A 90° pulse with time-proportional phase modulation (TPPM) was used with a duration of 0.6μs and a delay time of 3 s. The number of scans was 128. The reference for scanning was AlC13 (0.9 ppm) (Oluyinka et al., 2020).

## 3. Results and discussion

### 3.1. Effect of microwave power and time on the phase composition of fly ash

#### 3.1.1. XRD phase analysis of fly ash treated at different microwave powers

Fly ash samples were treated at varying microwave powers for the same duration, and XRD analysis was employed to investigate the phase composition.

The phase composition analysis revealed that the microwave activation method did not alter the phase evolution pattern in fly ash. However, under the same temporal conditions, a change in the intensity of the diffraction peak was observed. Extending the time, the main crystal phases in the 400 W sample are quartz, mullite, and calcium feldspar, and the content of the crystal phases was relatively the diffraction peak intensity and area did not change. In the 500 W sample, the relative content corresponding to the diffraction peak intensity and area of mullite and quartz increased and decreased slightly. In the 600 W sample, the content of the amorphous and some crystal phases continued to increase. In the 700 W sample, the content of the amorphous phase decreased, while the content of quartz and mullite increased slightly. In the 800 W sample, the content of mullite and quartz continued to increase. The decrease in mullite content may have been because high-power microwave treatment caused rapid temperature and pressure rise in a short period, leading to the crystallization of the amorphous phase and the appearance of new crystal phases (Ei-Feky et al., 2020). At the same time, the increased temperature was conducive to decomposing the inert component mullite, thereby reducing its formation. The microwave power also affected the phase composition of the treated fly ash. With the increase in microwave power, the content of some crystal phases in fly ash might have changed, and new crystal phases might have appeared. When the microwave time was short, the power reached 600 W. As the microwave time was extended, the power was increased to 700 W, the content of mullite and quartz reached a minimum, fewer crystal phases appeared, and the content of the amorphous phase was higher.

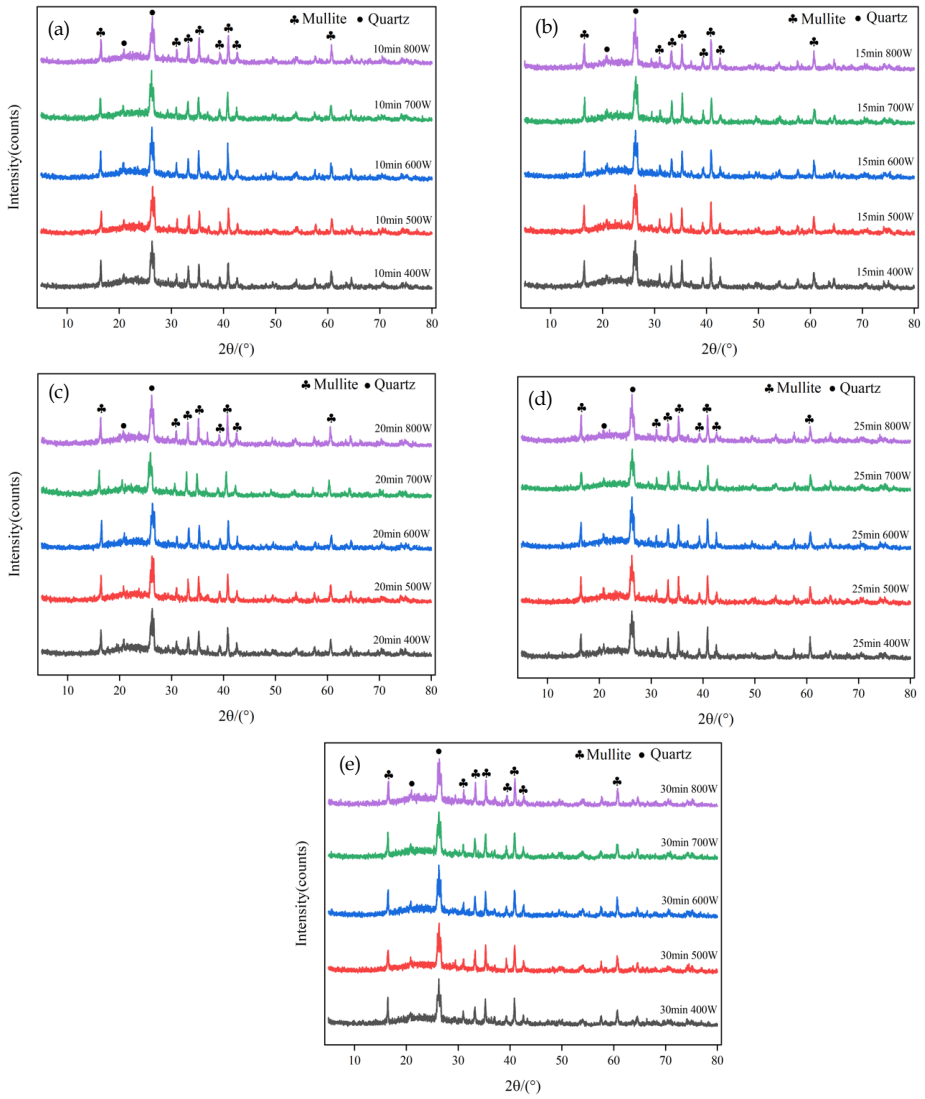


Fig. 4. XRD patterns of fly ash treated at different microwave powers for (a) 10 min, (b) 15 min, (c) 20 min, (d) 25 min, and (e) 30 min

### 3.1.2. Quantitative analysis of the adsorption performance of fly ash treated at different microwave powers

As observed in Fig. 5, it could be seen that the microwave power was optimal when it reached around 600 W. When the power was less than 600 W, the adsorption rate was lower. When the power exceeded 600 W, the adsorption rate decreased significantly, and local sintering conditions caused fluctuations and worse adsorption performance than the original ash. Based on this analysis, when the microwave power was low, the microwave energy could not fully penetrate the sample's interior, resulting in an unsatisfactory adsorption effect. The high-power microwave treatment produced higher temperature and pressure inside the fly ash in a short time than the low power, causing physical and chemical changes in the particles' interior and surface, removing many hydroxyl groups, and reducing adsorption performance (Tang et al., 2020). It could cause the local temperature to become too high, resulting in the sintering phenomenon, which blocked the internal pores, reduced porosity, and thus affected the adsorption performance. High power might have negative effects on the adsorption properties of fly ash by damaging the active sites, changing the microstructure, and affecting the surface properties. Therefore, when the microwave power reached 600 W, it reached the threshold for microwave power treatment of fly ash. Below 600 W, the sample surface temperature would slowly increase, and the microwave action time would be prolonged, which helped to protect the pore structure and improve the adsorption effect (Yakaboylu et al., 2019; Franus et al., 2019).

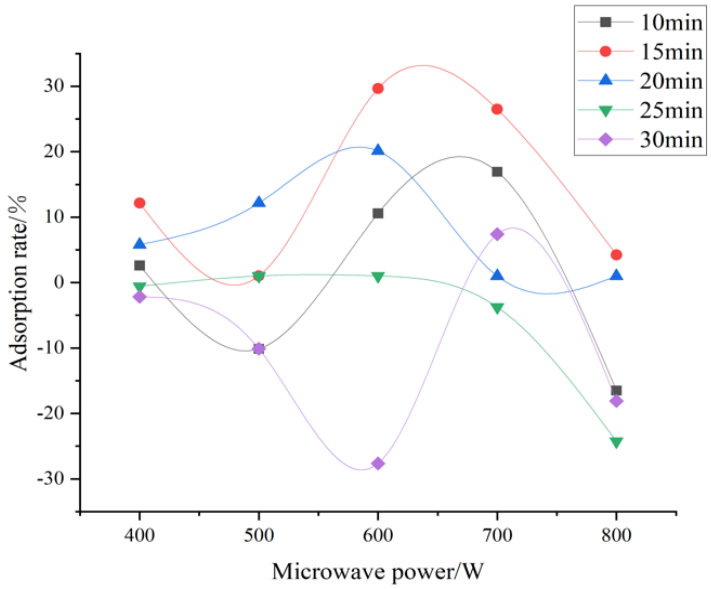


Fig. 5. Adsorption curves of fly ash treated at different microwave powers for the same duration

### 3.1.3. XRD phase analysis of fly ash treated by microwave for different durations

According to Fig. 6, when the power was fixed, the main crystal phases in the 10-minute sample were quartz, mullite, and calcium feldspar, and the content of the crystal phases remained relatively stable. In the 15-minute and 20-minute samples, the content of the amorphous phase and some crystal phases increased. In the 25-minute sample, the content of the amorphous phase decreased, while the content of quartz and mullite increased slightly. In the 30-minute sample, the content of the amorphous phase further decreased. The increase in microwave treatment time might have been due to physical and chemical reactions caused by microwave energy that destroyed the crystal structure. At the same time, the content of mullite changed slightly. The microwave time also affected the phase composition of the treated fly ash. With the increase in microwave time, microwave treatment could have promoted chemical bond breakage, and weakened the connection strength of silicon-oxygen bonds and aluminium-oxygen bonds, thus forming more amorphous substances. According to the XRD pattern, it could be observed that when the microwave time reached 15-20 minutes, the content of mullite and quartz was relatively low, and fewer crystal phases have appeared. In contrast, the content of the amorphous phase was higher.

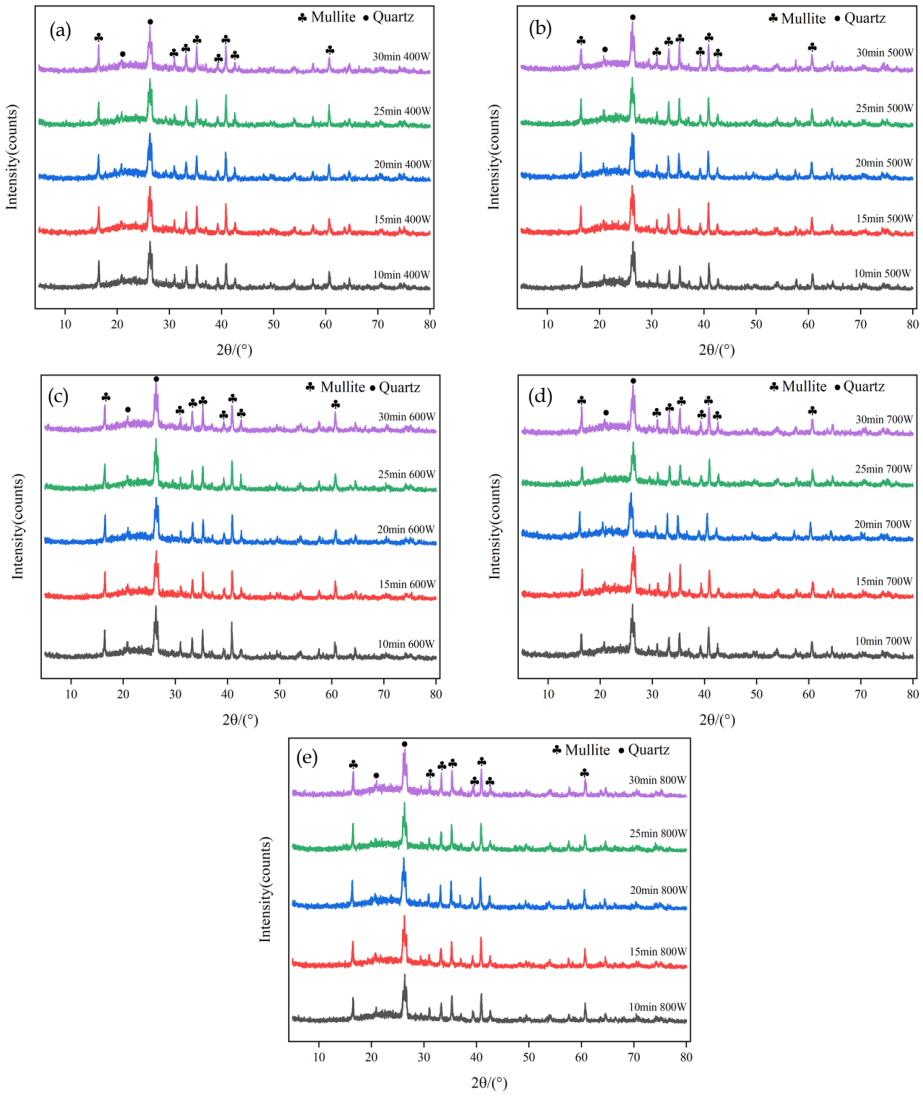


Fig. 6. XRD patterns of fly ash treated at different microwave times for (a) 400 W, (b) 500 W, (c) 600 W, (d) 700 W, and (e) 800 W

### 3.1.4. Quantitative analysis of adsorption performance of fly ash treated by microwave for different durations

As observed in Fig. 7, it could be seen that the adsorption rate generally reached its peak when the adsorption time reached 15 minutes. After 15 minutes, the adsorption performance continuously decreased. Before 15 minutes, the adsorption performance was slightly enhanced compared to the untreated fly ash, but the enhancement was weak. This analysis showed that microwave treatment heated the fly ash particles faster than traditional heating. If the adsorption time is too long, the adsorption activity center at the active site might have been denatured or deactivated, thus reducing its adsorption capacity to wastewater. There might have been phase change, melting, or sintering in the fly ash, resulting in the destruction or reduction of the pore structure, and these changes might have led to the reduction of the pore volume or the change of the pore size, which would have affected the adsorption capacity. Microwave treatment increases fly ash's adsorption rate of fly ash, but if the time is too short, the adsorption rate might not have reached its maximum value, thus affecting adsorption performance. Microwave digestion has a strong ability, could decompose the substances inside and on the surface of particles in a short time. However, if the treatment time was short, the fly ash particles might have become fragile and easily breakable, causing damage to the pore structure and affecting the adsorption performance. Therefore, it could be inferred that when the microwave time reached 15 minutes, it could have accelerated the chemical reactions and decomposition inside and on the surface

of particles quickly, thus forming more, larger and more uniform pore structures. These pores could have increased fly ash particles' specific surface area and pore volume, enhancing their adsorption performance (Hosseinpour et al., 2023). It could have also increased the broken surface of the particle surface, i.e., the reaction contact area, to enhance the activation effect and thus enhance the adsorption performance.

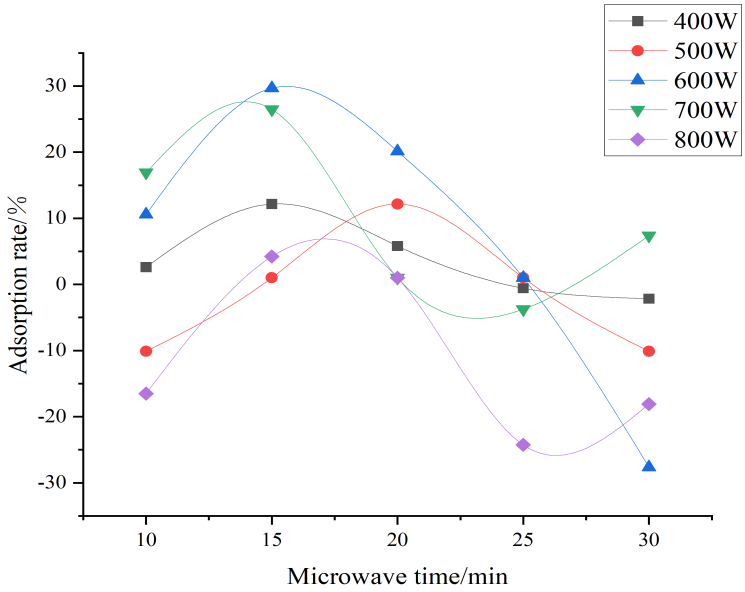


Fig. 7. Adsorption curves of fly ash treated by microwave for different durations at the same power

### 3.2. Effect of microwave power and time on the chemical bonds in fly ash

#### 3.2.1. FTIR analysis of fly ash treated at different microwave powers

To analyze the infrared absorption peaks of minerals and aluminosilicates, focusing on the mid to low-frequency region between 1400 and 400 $cm^{-1}$ was usually necessary. Therefore, comparing and analyzing the FTIR spectra of fly ash treated at different microwave powers in this region was crucial (Ghani et al., 2023).

As analyzed in Fig. 8, it could be seen that at the same treatment time, with the increase of microwave power, the absorption power at 400 W. At microwave treatment times of 25 min and 30 min, there was an increase in microwave power at 500 W and 600 W. This analysis showed that chemical bond breaking or formation might have occurred as the microwave power gradually increased, increasing the intensity of related infrared absorption peaks. As the heating process continued, the intensity of related infrared absorption peaks gradually decreased after reaching a certain threshold, possibly due to changes in the equilibrium state of chemical reactions. The absorption peak near 1100 $cm^{-1}$ in the Si-O-(Si, Al) anti-symmetric stretching vibration peak is related to the glass body, so its enhancement might have increased the amorphous phase content and improved the adsorption performance. The absorption peak near 460 $cm^{-1}$ reached its maximum at 500 W and 400 W after 10 min, 15 min, and 20 min of microwave treatment, respectively, and then decreased. When the microwave treatment time is 25 min and 30 min, the peak reached its highest point at 500 W. This vibrational peak was the bending vibration of Si-O-(Si) in quartz, and it reached its maximum value between 400~500 W, after which its relative content gradually decreased with increasing power. Therefore, it could be analyzed that the increase in microwave power led to the depolymerization of quartz. The Si-O-(Al) peak at 726 $cm^{-1}$ and the symmetric stretching vibration of Si-O-Si between 800~600 $cm^{-1}$ were less affected by microwave power and showed little change.

#### 3.2.2. FTIR analysis of fly ash treated at different microwave treatment times

As can be seen from Fig. 9, it was observed that at microwave powers of 400 W, 500 W, and 700W with the increase of treatment time, the absorption peak intensity near 1100 $cm^{-1}$ gradually increased and

then decreased. At 400 W, the absorption peak was enhanced at 10 and 15 min and then decreased with increasing time. At 700 W, the absorption peak is enhanced at 15 and 20 min, then decreases with increasing time. At microwave powers of 600 W and 800 W, there was little change in the peak before 15 min, and the peak intensity decreased significantly after 15 min. This analysis showed that prolonged microwave treatment time could cause decomposition or degradation reactions of compounds in fly ash, thereby changing their composition and structure. This change could lead to changes in the position, shape, and intensity of infrared absorption peaks. The experimental analysis showed that the glass body content might be higher at 15 min. The absorption peak near 460 $cm^{-1}$, which belonged to the bending vibration of Si-O-(Si) in quartz between 600~400 $cm^{-1}$, began to weaken after 15 min under microwave powers of 400 W, 600 W, and 800 W. There was little change before 15 min at microwave powers of 500 W and 700 W, then the peak increased. It was possible that when the microwave treatment time was too long, some quartz particles in the sample might undergo thermal decomposition, melting, or dissolution, leading to changes in their content (Luo et al., 2023). The Si-O-(Al) peak at 726 $cm^{-1}$ and the symmetric stretching vibration of Si-O-Si between 800~600 $cm^{-1}$ were less affected by the microwave treatment time due to their lower content.

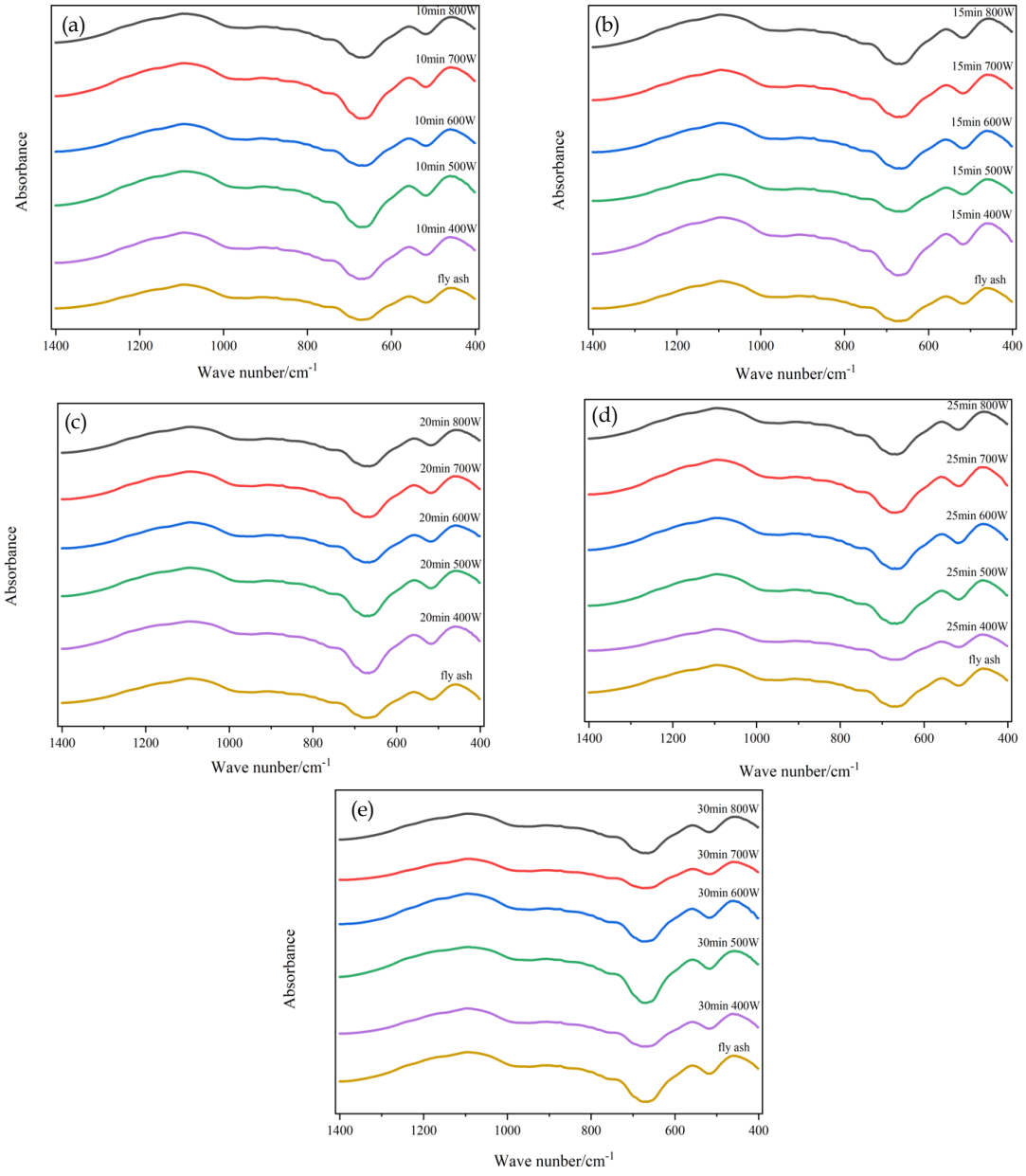


Fig. 8. FTIR spectra of fly ash treated at different microwave powers for (a) 10 min, (b) 15 min, (c) 20 min, (d) 25 min, and (e) 30 min

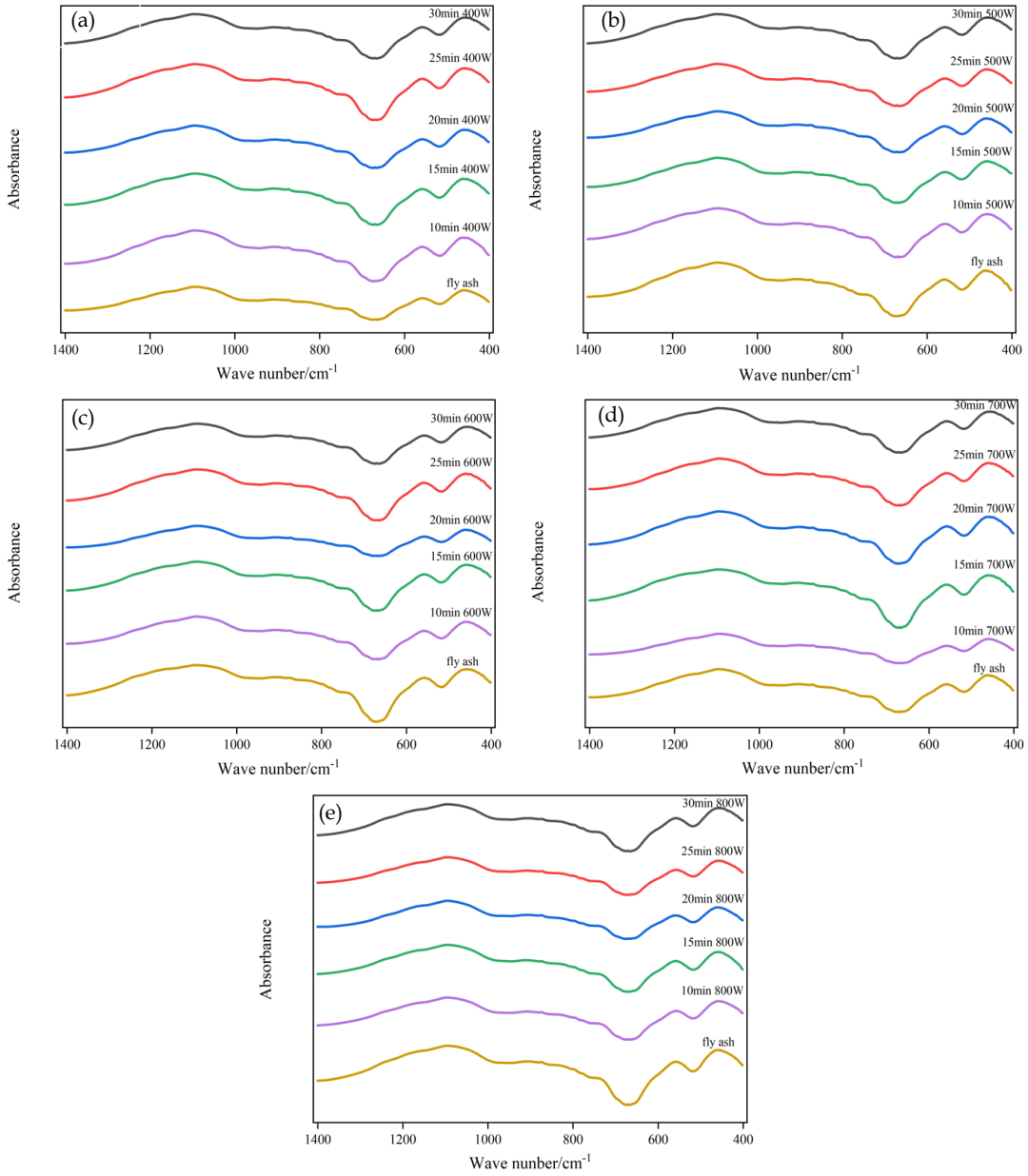


Fig. 9. FTIR spectra of fly ash treated at different microwave treatment times for (a) 400 W, (b) 500 W, (c) 600 W, (d) 700 W, and (e) 800 W

As can be seen from Fig. 9, it was observed that at microwave powers of 400 W, 500 W, and 700W with the increase of treatment time, the absorption peak intensity near 1100 $cm^{-1}$ gradually increased and then decreased. At 400 W, the absorption peak was enhanced at 10 and 15 min and then decreased with increasing time. At 700 W, the absorption peak is enhanced at 15 and 20 min, then decreases with increasing time. At microwave powers of 600 W and 800 W, there was little change in the peak before 15 min, and the peak intensity decreased significantly after 15 min. This analysis showed that prolonged microwave treatment time could cause decomposition or degradation reactions of compounds in fly ash, thereby changing their composition and structure. This change could lead to changes in the position, shape, and intensity of infrared absorption peaks. The experimental analysis showed that the glass body content might be higher at 15 min. The absorption peak near 460 $cm^{-1}$, which belonged to the bending vibration of Si-O-(Si) in quartz between 600~400 $cm^{-1}$, began to weaken after 15 min under microwave powers of 400 W, 600 W, and 800 W. There was little change before 15 min at microwave powers of 500 W and 700 W, then the peak increased. It was possible that when the microwave treatment time was too long, some quartz particles in the sample might undergo thermal decomposition, melting,

or dissolution, leading to changes in their content (Luo et al., 2023). The Si-O-(Al) peak at 726 $cm^{-1}$ and the symmetric stretching vibration of Si-O-Si between 800~600 $cm^{-1}$ were less affected by the microwave treatment time due to their lower content.

### 3.3. Effect of microwave treatment on the morphology of fly ash

As shown in Fig. 10, the surface of the smooth fly ash had irregular granular material, and depolymerized mullite and quartz were adsorbed on the surface; this was different from the fly ash without microwave treatment in Fig. 2. This indicated that microwave treatment could induce changes in the morphology of fly ash, resulting in surface irregularities and fractures in some particles. Microwave treatment induced the fragmentation of fly ash particles and dissociation of quartz and mullite phases, leading to voids and cracks in the hollow fly ash particles (Ioana et al., 2022). The fractures of fly ash particles could increase their specific surface area and enhance the reactivity. On the other hand, continuous microwave treatment induced polarization of the quartz and mullite phases in fly ash, resulting in cleavage of the Al-O and Si-O bonds. This promoted the partial melting of fly ash and its transformation into the amorphous phase, facilitating the conversion of dissociated quartz and mullite phases. As pozzolanic activity was mainly attributed to the hydration reaction of the amorphous phase, increasing this phase could accelerate the early-stage reaction rate and enhance the activity of fly ash (Al-Dahri et al., 2022).

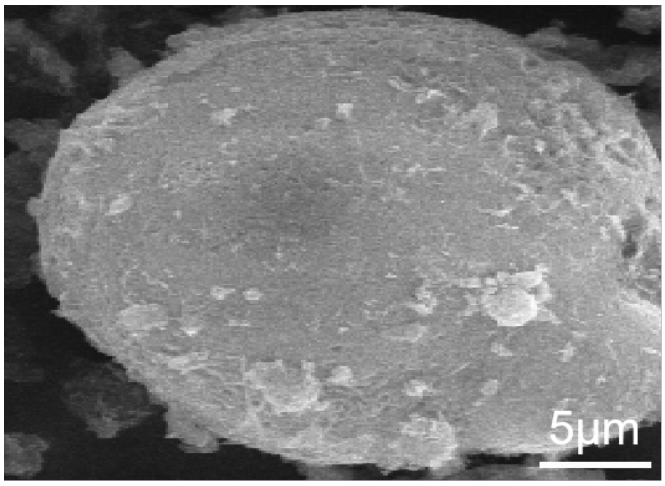


Fig. 10. SEM morphology of pre-treated fly ash

### 3.4. XRD-Rietveld refinement semi-quantitative analysis and infrared peak fitting semi-quantitative analysis

XRD-Rietveld refinement semi-quantitative analysis and infrared peak fitting semi-quantitative analysis were carried out on fly ash treated at microwave power and time with results from phase and infrared analyses and adsorption performance tests. Through adsorption experiment, phase and strength analysis, and spectral analysis, the samples treated at 600 W for 10 min, 15 min, 20 min, 25 min, and 30 min were selected for analysis (Singh et al., 2023).

#### 3.4.1. XRD-Rietveld refinement semi-quantitative analysis

The Rietveld full-pattern fitting results of fly ash before and after microwave treatment are shown in Figs. 11 and 12.

After multi-phase fitting, the proportion between different crystal phases could be obtained. The quartz, mullite, and amorphous phases in fly ash could be calculated by comparing the content of zinc oxide doped internally. The semi-quantitative analysis results of various phases in fly ash are presented in Table 2. As shown in Table 2, after the microwave treatment, there was a slight decrease in the quartz and mullite content, while the mullite and amorphous phase increased inversely. The decrease in mullite content and the relative increase in amorphous phase content indicated that mullite may have undergone depolymerization, and the glassy structure on the surface of fly ash had been destroyed,

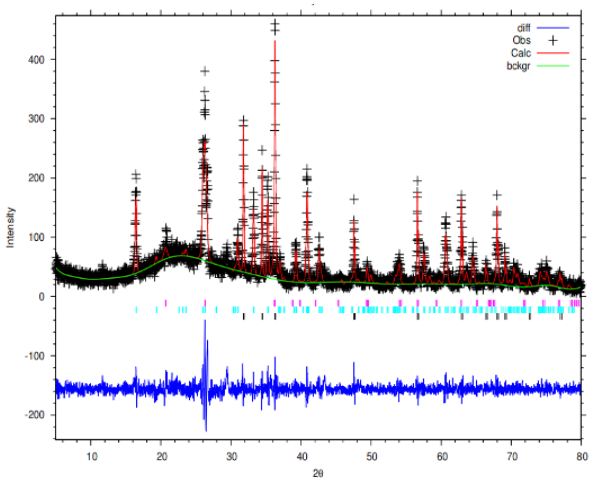


Fig. 11. The Rietveld whole pattern fitting result of the fly ash is shown in the Fig., where the experimental values (crosses) are fitted to the calculated values (solid line)

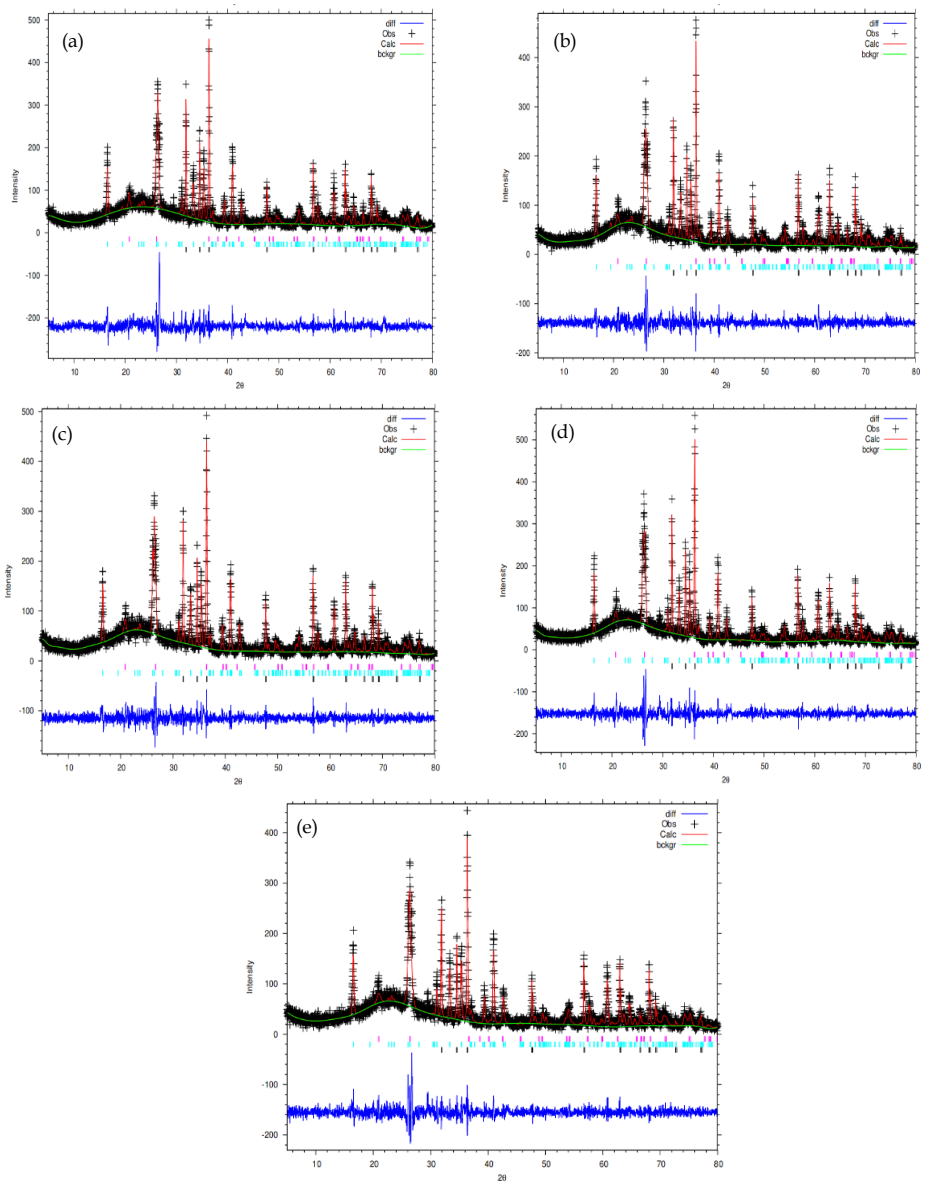


Fig. 12. Rietveld whole-pattern fitting results of fly ash under microwave for (a) 600 W-10 min, (b) 600 W-1 5min, (c) 600 W-20 min, (d) 600 W-25 min and (e) 600 W-30min

leading to an increase in the amorphous phase content. At the same time, with the prolongation of microwave time, the content of quartz continued to decrease, indicating that the prolonged high temperature might reduce the crystallinity of quartz (Marjanović et al., 2014).

Table 2. Rietveld fitting of the relative content of each phase in fly ash under different microwave conditions

| Samples | Mullite | Quartz (%) | Amorphous (%) |
|---|---|---|---|
| Fly ash | 45.9 | 17.64 | 36.46 |
| 600 W 10 min | 43.55 | 17.1 | 39.35 |
| 600 W 15 min | 41.8 | 12.02 | 46.18 |
| 600 W 20 min | 40.38 | 14.7 | 44.92 |
| 600 W 25 min | 44.36 | 9.3 | 46.34 |
| 600 W 30 min | 45.72 | 11.04 | 43.24 |

### 3.4.2. Infrared peak fitting semi-quantitative analysis

Fig. 13 shows the fitted spectrum. According to the analysis of the peak areas in the infrared peak fitting semi-quantitative analysis spectrum, the relative percentage content of Si-O-(Si, Al) chemical bonds between 1300~900 $cm^{-1}$ was between 49.47% and 56.92%, all of which were higher than that of the original fly ash. Compared with the original fly ash, the proportion of peak area gradually increased until 15 min and then gradually decreased. The relative percentage content of Si-O-(Si) chemical bonds between 600~400 $cm^{-1}$ is between 17.5% and 28.9%, with a relatively even proportion of peak area at 600 W and a significant decrease at 15 min. The semi-quantitative analysis of infrared peak fitting showed the change in the peak area of the spectrum, as shown in Table 3.

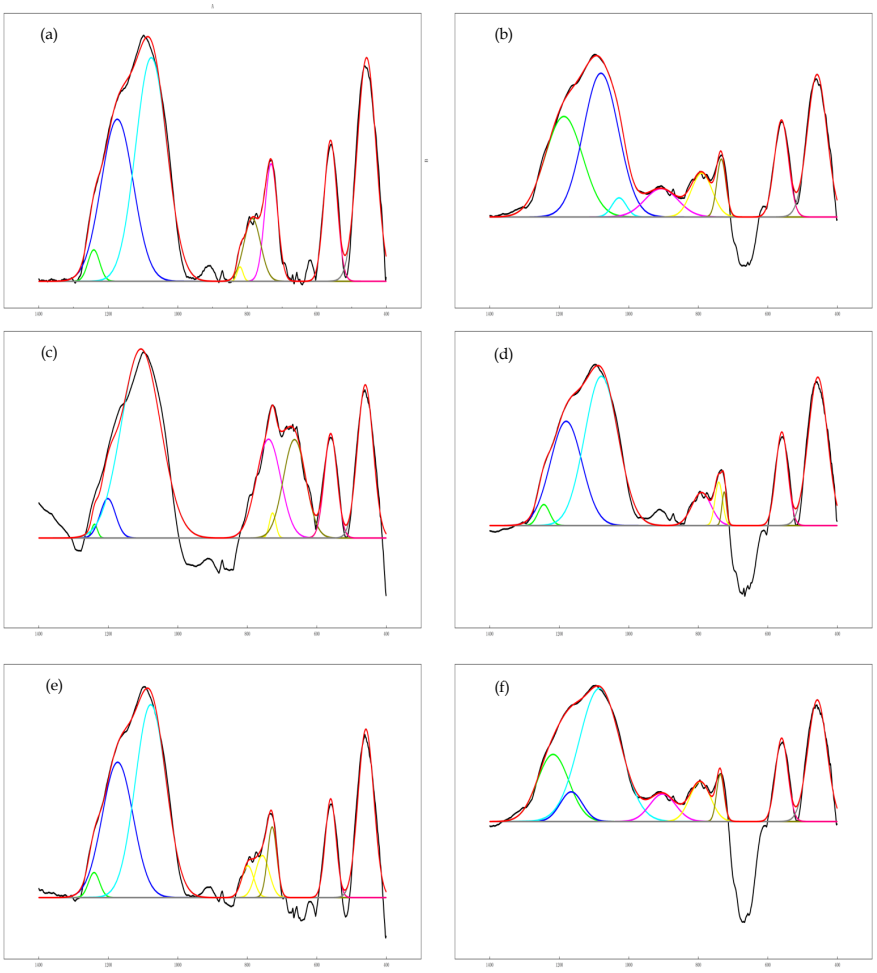


Fig. 13. Infrared semi-quantitative analysis chart of fly ash treated with microwave for (a) original fly ash, (b) 10 min, (c) 15 min, (d) 20 min, (e) 25 min, and (f) 30 min

Table 3. The peak area of the main absorption under different conditions

| Samples | Peak position ($cm^{-1}$) | Peak area ratio (%) | Peak position ($cm^{-1}$) | Peak area ratio (%) |
|---|---|---|---|---|
| Fly ash | 1300~900 | 47.98 | 600~400 | 28.14 |
| 600 W 10 min | 1300~900 | 49.47 | 600~400 | 25.8 |
| 600 W 15 min | 1300~900 | 54.01 | 600~400 | 17.5 |
| 600 W 2 min | 1300~900 | 51.64 | 600~400 | 28.9 |
| 600 W 25 min | 1300~900 | 56.92 | 600~400 | 25.14 |
| 600W 30 min | 1300~900 | 50.21 | 600~400 | 25.36 |

### 3.5. Specific surface area test

By using a JW-BK112 type surface area and aperture distribution tester, degassing and impurity removal of raw ash, 600 W-10 min, 600 W-15 min, 600 W-20 min, 600 W-25 min, and 600 W-30 min fly ash samples were carried out. After degassing treatment, adsorption and desorption experiments were carried out. Nitrogen was selected as the adsorbent gas, and the test temperature was -195.79°C of liquid nitrogen evaporation temperature. The specific surface area and porosity were tested, and various parameters related to pore structure were obtained, including the specific surface area of fly ash (BET method was used), micropore volume average pore size, and so on. The test results are shown in Table 4.

Table 4. Specific surface area and porosity under different conditions

| Samples | Specific surface area ($m^2 \cdot g^{-1}$) | Pore volume ($cm^3 \cdot g^{-1}$) | Average pore size (nm) | Adsorption average pore diameter (nm) |
|---|---|---|---|---|
| Fly ash | 2.436 | 0.013 | 13.099 | 8.788 |
| 600 W 10 min | 2.762 | 0.013 | 13.094 | 9.444 |
| 600 W 15 min | 3.122 | 0.015 | 14.358 | 10.327 |
| 600 W 20 min | 3.058 | 0.015 | 15.069 | 10.850 |
| 600 W 25min | 2.793 | 0.015 | 16.064 | 10.851 |
| 600 W 30 min | 2.813 | 0.016 | 15.541 | 10.728 |

As shown in Table 4, the specific surface area increased and then decreased with time, which was higher than the original fly ash. The specific surface area reached a maximum of 3.122 $m^2/g$ at 15 min of microwave treatment. The pore volume increased continuously with microwave treatment time, while the average pore size first increased and then became stable. From this analysis, the specific surface area and pore volume of fly ash increased in the early stage of microwave heating because the volatilization of some volatile components and the decomposition and removal of oxygen-containing functional groups generated new pore structures, promoting micropore development. However, as the heating time increases, microwave radiation will erode the existing pore structure, and some frameworks will begin to collapse, increasing pore size. Because the specific surface area of fly ash was a key factor affecting its adsorption efficiency, the larger the specific surface area of fly ash, the more adsorption sites could be provided, which increased the rate and amount of adsorption reaction (Kunecki et al., 2023). Therefore, it was vital to adsorb substances such as ammonia nitrogen.

As shown in Fig. 14, the microwave-treated fly ash samples' nitrogen adsorption-desorption isotherms were above those of raw fly ash. The adsorption increased in the low-pressure region and entered a relatively stable increasing zone. When the relative pressure reached the middle-pressure region, the adsorption increased significantly. When the relative pressure reached the high-pressure region, adsorption increased sharply, representing the characteristics of micropore adsorption, mesopore adsorption, and macropore adsorption. At the highest point of adsorption, under the same pressure, the adsorption amount was higher at 15 min and 20 min, followed closely by 30 min, 25 min, and 10 min, all of which had a significant increase in adsorption compared to raw fly ash (Jain et al., 2022; Elkarrach et al., 2023).

### 3.6. Nuclear magnetic resonance (NMR) testing

Solid-state nuclear magnetic resonance was an essential tool for analyzing the local magnetic environ-

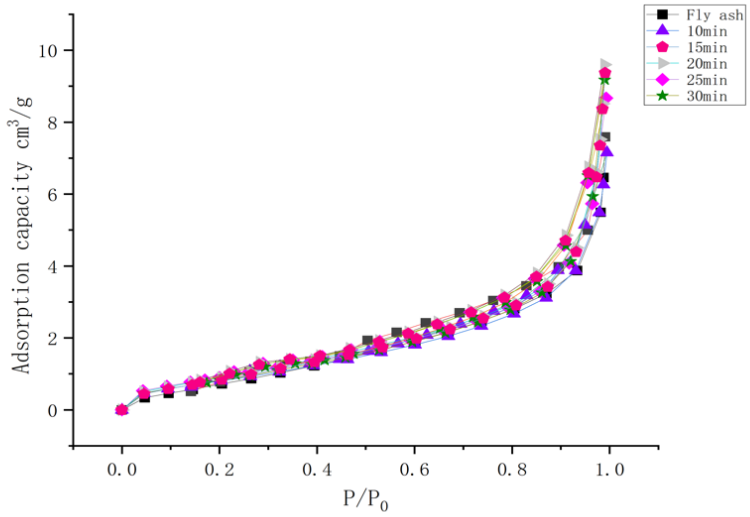


Fig.14. Nitrogen adsorption-desorption isotherms of raw and microwave-treated fly ash

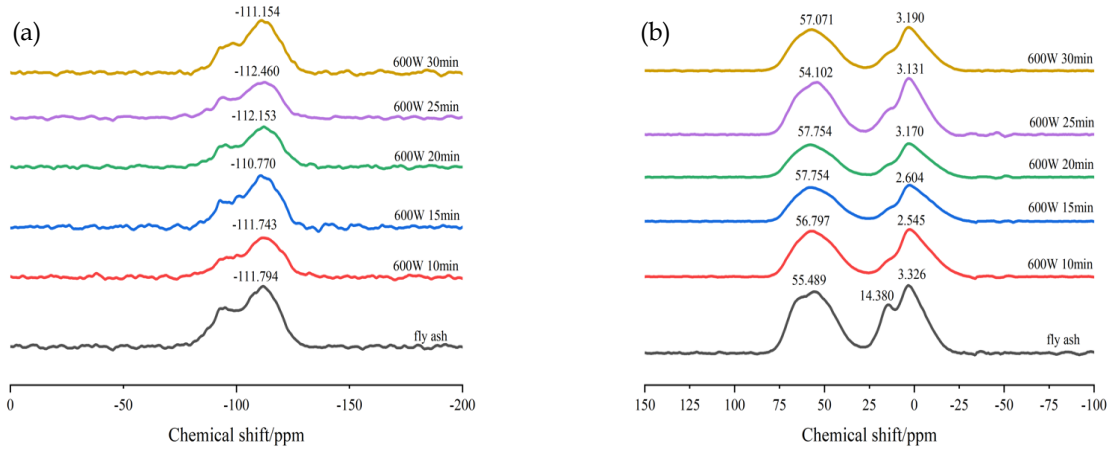


Fig. 15. MAS NMR spectra of fly ash before and after microwave treatment for (a) $^{29}Si$ and (b) $^{27}Al$

ments of nuclei in mineral structures. A deeper understanding of the microstructural evolution of fly ash during the microwave process could be obtained through $^{29}Si$ and $^{27}Al$ MAS NMR spectra (Medykowska et al., 2022). This method provided a direct approach that could be used to explore the microstructure and chemical reaction mechanisms of solid materials.

As shown in Fig. 15, the fly ash belonged to the framework structure before and after microwave treatment. In the early stage of microwave treatment, the intensity of the $Q^4Si$ signal in the $^{29}Si$ spectrum decreased, indicating that the microwave caused crystal defects, distortions, and deformations in the fly ash, thereby reducing its orderliness. Among them, the signal intensity was higher, and the peak was broader at 600 W and 15 min with time, the chemical shift began to change, showing a trend of first increasing and then decreasing, reaching a maximum of -110.770 ppm at 600 W and 15 min. It indicated a significant structural change and an increase in the degree of amorphization at this time. The peak curves of the $^{27}Al$ spectrum before and after microwave treatment had a similar shape, indicating that the coordination state types of $Al^{3+}$ in the structure under various microwave conditions were similar. However, the proportions of each coordination state that constitutes $Al^{3+}$ were different. With the change in microwave time, the peak value of the $^{27}Al$ spectrum line shifted, indicating that the structural status of aluminium-oxygen in the fly ash changed accordingly (Alakent et al., 2022).

In this study, DMFIT software was used to perform peak fitting analysis on the samples' NMR $^{29}Si$ and $^{27}Al$ spectra, and the fitting results obtained were in good agreement with the original spectra. The results of the peak fitting are shown in Figs. 16 and 17. The relative contents of the three coordination states ($[AlO_4]$, $[AlO_5]$, and $[AlO_6]$) in the $^{27}Al$ spectrum and the four coordination states ($Q^1$, $Q^2$, $Q^3$, and

$Q^4$) in the $^{29}Si$ spectrum were obtained through integration calculations of the peak areas, as shown in Table 4 and 5. As shown in Table 5, $Al^{3+}$ in fly ash mainly exists in the form of [$AlO_4$] and [$AlO_6$], with a relatively small proportion of [$AlO_5$]. The [$AlO_4$] coordination state showed a gradually increasing trend and could form a unified network with [$SiO_4$], strengthening the polymerization degree (Chen et al., 2022). The content of [$AlO_5$] and [$AlO_6$] formed by $Al^{3+}$ in the structure would increase accordingly, causing a decrease in the polymerization degree of the aluminium-oxygen network. It could be seen from Table 5 that the content of [$AlO_5$] and [$AlO_6$] was the highest at 15 minutes, indicating a lower polymerization degree at this time (Aelst et al., 2014) This occurred because microwave heating broke the silicon-oxygen network bond in fly ash, and the coordination state formed by aluminum ions in the silicon-oxygen network was closely related to the amount of free oxygen. Insufficient free oxygen led to

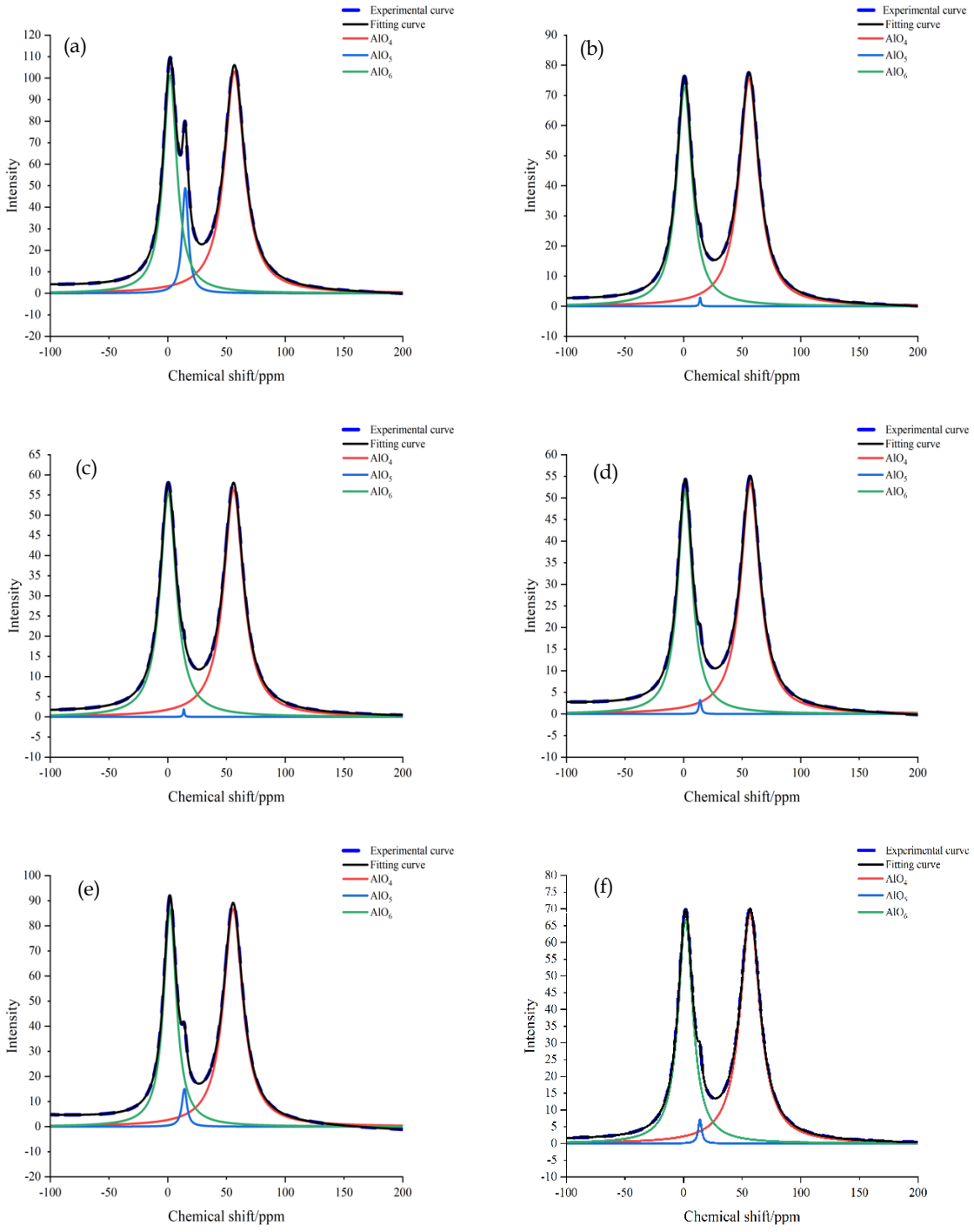


Fig. 16. Peak fitting of the $^{27}Al$ spectrum and after microwave treatment for (a) original fly ash, (b) 10 min, (c) 15 min, (d) 20 min, (e) 25 min, and (f) 30 min

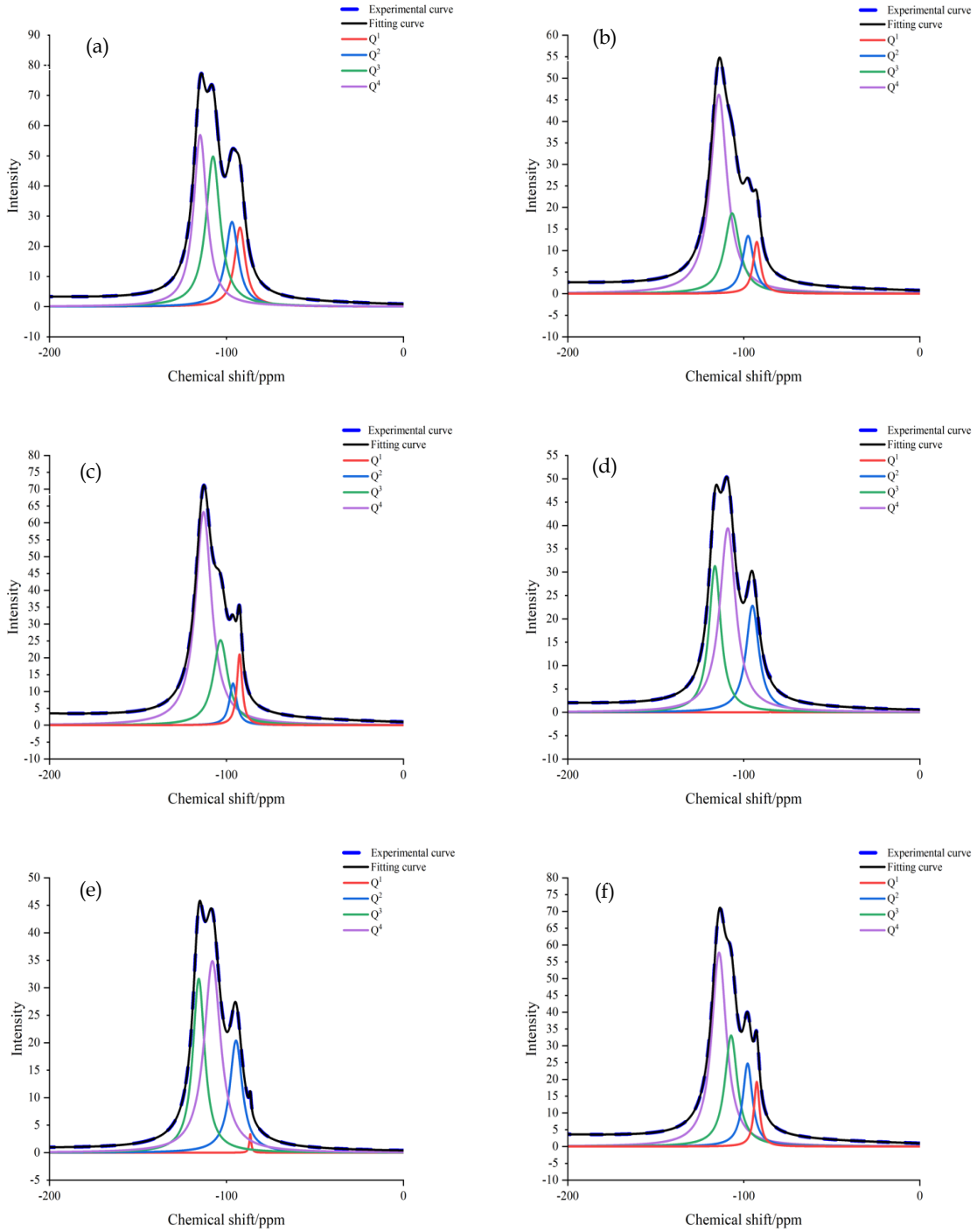


Fig. 16. Peak fitting of the $^{29}Si$ spectrum and after microwave treatment for (a) original fly ash, (b) 10 min, (c) 15 min, (d) 20 min, (e) 25 min, and (f) 30 min

the formation of $[AlO_4]$ by $Al^{3+}$, which is inadequate for establishing a network with $[SiO_4]$. Consequently, the $Al^{3+}$ peak shifts, causing changes in the structure of the silicon-oxygen network and resulting in a gradual decrease in polymerization.

As shown in Table 6, the sum of the proportions of $Q^3$ and $Q^4$ before and after microwave treatment was both higher than 67%, indicating that silicon-oxygen tetrahedra in fly ash mainly exist in the form of 3-4 bridging oxygen, and the silicon-oxygen network was between layered and framework structures. With time, the integral contents of $Q^1$ and $Q^2$ decreased significantly at 10 minutes and 15 minutes. The proportion of $Q^3$ and $Q^4$ increased after 10 minutes, increasing the connectivity and polymerization degree of the silicon-oxygen network in the sample. The connectivity of the silicon-oxygen network in

the structure was thus strengthened. After 15 min, the proportion of $Q^3$ and $Q^4$ was the lowest, and the proportion of $Q^1$ and $Q^2$ increased, indicating a decrease in the polymerization degree (Nie et al., 2012; Bernard et al., 2023).

Table 5. Calculated peak areas of the 27Al fitting before and after microwave treatment

| Samples | $[AlO_6]$ (%) | $[AlO_5]$ (%) | $[AlO_4]$ (%) |
|---|---|---|---|
| Fly ash | 37.20 | 8.31 | 54.49 |
| 600 W 10 min | 43.55 | 0.17 | 56.28 |
| 600 W 15min | 45.02 | 0.12 | 54.86 |
| 600 W 20min | 42.54 | 0.45 | 57.01 |
| 600 W 25min | 39.25 | 2.73 | 58.02 |
| 600 W 30 min | 42.17 | 1.10 | 56.73 |

Table 6. Calculated peak areas of the 29Si fitting before and after microwave treatment

| Samples | $Q^1$ (%) | $Q^2$ (%) | $Q^3$ (%) | $Q^4$ (%) |
|---|---|---|---|---|
| Fly ash | 15.72 | 16.31 | 32.33 | 35.64 |
| 600 W 10 min | 7.06 | 11.54 | 21.78 | 59.62 |
| 600 W 15 min | 6.82 | 15.10 | 20.55 | 57.83 |
| 600 W 20 min | 0.54 | 19.20 | 31.91 | 48.35 |
| 600 W 25 min | 0.02 | 24.11 | 31.88 | 43.99 |
| 600 W 30 min | 6.80 | 14.96 | 25.88 | 52.96 |

## 4. Conclusions

The improvement of the performance of fly ash after microwave pretreatment was mainly due to the breakage of chemical bonds, which was mainly caused by the high-frequency electric field generated by the microwave, resulting in uniform heating of the material, increased collisions and disorderly movement of molecules after absorption of energy, leading to an increase in surface area and an increase in utilization efficiency. The researchers in this study characterized the microwave pretreatment of fly ash using traditional analysis methods and semi-quantitative analysis. It was found that microwave pretreatment did not significantly affect the phase of fly ash. However, it did change the adsorption performance by increasing the adsorption rate by 28%. The microwave pretreatment also caused the breaking of chemical bonds and increased the specific surface area of the fly ash. Moreover, the microstructure changes resulted in the depolymerization of quartz and mullite. Through semi-quantitative analysis, the optimal microwave condition was 600 W for 15 min. Under these conditions, the content of the amorphous phase increased significantly. the infrared absorption peak area also increased. Furthermore, the degree of polymerization of the silica network, as observed in the $^{29}Si$ and $^{27}Al$ spectra, decreased after 15 min of microwave pretreatment. To further improve performance, future investigations should explore the effects of combining microwave pretreatment of fly ash with other pretreatment methods.

## Acknowledgments

This research was funded by the National Natural Science Foundation of China (Grant No. 52004091), and the Natural Science Foundation of Hebei Province (Grant No. E2019209494).

## References

AELST, J.V., HAOUAS, M., GOBECHIYA, E. and HOUTHOOFD, K., 2014. *Hierarchization of USY Zeolite by $NH_4OH$. A Postsynthetic Process Investigated by NMR and XRD.* The Journal of Physical Chemistry, C. Nanomaterials and Interfaces, 118(39), 22573-22582.

ALAKENT, B., KAYAÖZKIPER, K., and SOYERUZUN, S., 2022. *Global interpretation and generalizability of boosted regression models for the prediction of methylene blue adsorption by different clay minerals and alkali activated materials.* Chemosphere, 308(P1), 136248.

AL-DAHRI, T., ABDULRAZAK, A., and ROHANI, S., 2022. *Preparation and characterization of Linde-type A zeolite (LTA) from coal fly ash by microwave-assisted synthesis method: its application as adsorbent for removal of anionic dyes.* International Journal of Coal Preparation and Utilization, 42(7).

BERNARD, E., LOTHENBACH, B., GERMAN, A., and RENTSCH, D., 2023. *Effect of aluminate and carbonate in magnesia silicate cement.* Cement and Concrete Composites, 139, 105010.

CHEN, C.Y., ZHONG, C., ZHANG, Y., and LI, A., 2022. *Structural and dynamic properties of $MgO–Al_2O_3–SiO_2$ glasses from molecular dynamics simulations and NMR.* Ceramics International, 48(15).

CHEN, W., SONG, G.Q., LIN, Y.Y., and QIAO, J.T., 2022. *Synthesis and catalytic performance of Linde-type A zeolite (LTA) from coal fly ash utilizing microwave and ultrasound collaborative activation method.* Catalysis Today, 397-399.

DAS, D., and ROUT, P.K., 2023. *A review of coal fly ash utilization to save the environment.* Water, Air, & Soil Pollution, 234(2), 1-23.

DINDI, A., DANG, V., QUANG, D.V., and VEGA, L.F., 2019. *LOURDES F. Vega, R.M. Abu-Zahra. Applications of fly ash for $CO_2$ capture, utilization, and storage*. Journal of $CO_2$ Utilization, 29, 82-102.

EI-FEKY, M.S., KOHAIL, M., MAHER, A., and SERAG, M.I., 2020. *Effect of microwave curing as compared with conventional regimes on the performance of alkali activated slag pastes.* Construction and Building Materials, 233(117268).

ELKARRACH, K., OMOR, A., ATIA, F., and LAIDI, O., 2023. *Mohamed, Merzouki Mohammed. Treatment of tannery effluent by adsorption onto fly ash released from thermal power stations: Characterisation, optimization, kinetics, and isotherms.* Heliyon, 9(4), e12687.

FRANUS, M., PANEK, R., MADEJ, J., and FRANUS, W., 2019. *The properties of fly ash derived lightweight aggregates obtained using microwave radiation*. Construction and Building Materials, 227(116677).

GHANI, S.M., RABAT, N.E., RAHIM, A.R.A., JOHARI, K., SIYAL, A.A., and KUMERESEN, R., 2023. A*BDUL Rahim Abdul Rahman, Amine Infused, et al. Fly ash grafted acrylic acid/acrylamide hydrogel for carbon dioxide ($CO_2$) adsorption and its kinetic analysis*. Gels, 9(3).

GOPALAN, A., RAMESH, S., NIRMALA, P., GOVINDARAJ, D.R., SAHOO, S., SHIFANI, S.A., and JAYADHAS, S. A., 2022. *Investigation of insulation properties using microwave nondevastating methodology to predict the strength of polymer materials.* Advances in Materials Science and Engineering, 3, 1-9.

GULTEKIN, A. and RAMYAR, K., 2023. *Investigation of high-temperature resistance of natural pozzolan-based geopolymers produced with oven and microwave curing.* Construction and Building Materials, 365(2), 130059.

HAN, Q.C., TANG, J. and LU, J.G.Z., 2003. *Standard specification for fly ash and raw or calcined natural pozzolan for use as a mineral admixture in concrete (ASTMC 618)*. Coal Ash China, 2, 44–45.

HOSSEINPOUR, S., MEHRIZI, M.H., HASHEMIPOUR, H., and FARPOOR, M.H., 2023. *Adsorptive removal of phosphorus from aqueous solutions using natural and modified coal solid wastes*. Water Science and Technology: A Journal of the International Association on Water Pollution Research, 87(6).

IOANA, A., PAUNESCU, L., NICOLAE, C., POLLIFRONI, M., DEONISE, D., and PETCU, F.S., 2022. *Glass foam from flat glass waste produced by the microwave irradiation technique.* Micromachines, 13(4), 550.

JAIN, S., BANTHIA, N., and TROCZYNSKI, T., 2022. *Conditioning of simulated cesium radionuclides in NaOH-activated fly ash-based geopolymers*. Journal of Cleaner Production, 380, 134984.

KUNECKI, P., WDOWIN, M., and HANC, E., 2023. *Fly ash-derived zeolites and their sorption abilities in relation to elemental mercury in a simulated gas stream.* Journal of Cleaner Production, 391, 136181.

LUO, S.Q., GE, Y.L., and PAN, C.G., 2023. *Microstructures of fly ash activated by microwave and early properties of flyash-cement slurry*. Materials Reports, 1-17.

LV, Y., 2018. *Experience in the operation of water chemical titration.* Northern Chinese Fisheries, (02), 17-19.

MAJID, B. 2021. *Application of fly ash and fine limestone powder in cement and concrete.* Journal of Progress in Civil Engineering, 3(7).

MA, P.C., LI, X., WEN, Z.Y., MENG, F.H., and LI, Z., 2021. *Research progress on active excitation and mechanism of fly ash*. Inorganic Chemicals Industry, 53(10), 28-35.

MARJANOVIĆ, N., KOMLJENOVIĆ, M., BAŠČAREVIĆ, Z., and NIKOLIĆ, V., 2014. I*mproving reactivity of fly ash and properties of ensuing geopolymers through mechanical activation.* Construction and Building Materials, 57, 151-162.

MATHAPATI, M.K., AMATE, K., PRASAD, D., JAYAVARDHANA, M.L., and RAJU, T.H., 2021. *A review on fly ash utilization.* Materials Today Proceedings, 50(2).

MA, X.Y., NIE, Y.M., CHEN, Y., LI, T., HUANG, H., LIU, S.X., WANG, L., and WANG, L., 2022. *Synthesis of fly ash-based zeolite molecular sieve and research status of its structural properties*. Metal Mine, (08), 82-93.

MEDYKOWSKA, M., WIŚNIEWSKA, M., SZEWCZUK, K.K., and PANEK, R., 2022. *Simultaneous removal of inorganic and organic pollutants from multicomponent solutions by the use of zeolitic materials obtained from fly ash waste*. Clean Technologies and Environmental Policy, 25(3).

MOISILI, P.E. and JEN, T.C., 2022. *Microwave-assisted sol–gel template-free synthesis and characterization of silica nanoparticles obtained from South African coal fly ash.* Nanotechnology Reviews, 11(1), 3042-3052.

NGUYEN, H.T., NGUYEN, H.T., and AHMED, S.F., 2023. *Emerging waste-to-wealth applications of fly ash for environmental remediation: A review*. Environmental Research, 227:115800.

NIE, Y.M., XIA, M.H., BAI, L.M., LIU, S.X., ZHANG, J.X., and NIU, F.S., 2012. *Analysis method of ~(27)Al, ~(29) Si solid high-resolution nuclear magnetic resonance pattern analysis of silicon (aluminum) salt mineral crystals*. Bulletin of the Chinese Ceramic Society, 31(05), 1200-1203.

OLUYINKA, O.A., PATEL, A.V., SHAH, B., and BAGIA, M., 2020. *Microwave and fusion techniques for the synthesis of mesoporous zeolitic composite adsorbents from bagasse fly ash: sorption of p-nitroaniline and nitrobenzene*. Applied Water Science, 10(12).

PANITSA, O.A., KIOUPIS, D., and KAKALI, G., 2022. *Thermal and microwave synthesis of silica fume-based solid activator for the one-part geopolymerization of fly ash.* Environmental Science and Pollution Research International, 29(39).

PRAIPIPAT, P., NGAMSURACH, P., and ROOPKHAN, N., 2023. *Zeolite A powder and beads from sugarcane bagasse fly ash modified with iron(III) oxide-hydroxide for lead adsorption*. Scientific Reports, 13(1).

RUSĂNESCU, C.O., and RUSĂNESCU, M., 2023. *Application of fly ash obtained from the incineration of municipal solid waste in agriculture*. Applied Sciences, 13(5), 3246.

SHI, S., LI, H., ZHOU, Q. Z., ZHANG, H.Z., and BAI, Y., 2023. *Alkali-activated fly ash cured with pulsed microwave and thermal oven: A comparison of reaction products, microstructure and compressive strength.* Cement and Concrete Research, 166(8).

SINGH, K., KUMAR, A., SINGH, A.K., and AGARWAL, A., 2023. *Fly ash and $TiO_2$ modified fly ash as adsorbing materials for effective removal of methylene blue and malachite green from aqueous solutions.* Journal of the Indian Chemical Society, 100(3), 100942.

TANG, T., CAI, L.X., YOU, K., and LIU, M., 2020. *Effect of microwave pre-curing technology on carbide slag-fly ash autoclaved aerated concrete (CS-FA AAC): Porosity rough body formation, pore characteristics and hydration products.* Construction and Building Materials, 263(29), 120112.

UM, N. and JEON, T.W., 2021. *Pretreatment method for the utilization of the coal ash landfilled in ash ponds. Process* Safety and Environmental Protection, 153(9).

VALEEV, D. and KONDRATIEV, A., 2022. *Current state of coal fly ash utilization: Characterization and application.* Materials, 16(1), 27.

YAKABOYLU, G.A., BAKER, D., WAYDA, B., and SABOLSKY, K., 2019. *Microwave-assisted pretreatment of coal fly ash for enrichment and enhanced extraction of rare-earth elements*. Energy & Fuels, 33(11).

YILDIZ, K., and ATAKAN, M., 2020. *Improving microwave healing characteristic of asphalt concrete by using fly ash as a filler*. Construction and Building Materials, 262(120448), 1-9.

ZHANG, L.J., YUAN, H., PENG, L., PENG, J.H., LI, S.W., CHEN, K.H., YIN, S.H., ZHANG, L.B., 2020. *Comparison of microwave and conventional heating routes for kaolin thermal activation.* Journal of Central South University, 27, 2494-2506.

ZHOU, Q., JIANG, X.G., QIU, Q. L., ZHAO, Y.M., and LONG, L., 2022. Ling. *Synthesis of high-quality NaP1 zeolite from municipal solid waste incineration fly ash by microwave-assisted hydrothermal method and its adsorption capacity.* The Science of the Total Environment, 855(8), 158741.

ZUMA, M.C., NOMNGONGO, P.N. and MKETO, N., 2021. *Simultaneous determination of REEs in coal samples using the combination of microwave-assisted ashing and ultrasound-assisted extraction methods followed by ICP-OES analysis.* Minerals, 11(10), 1103.